SPE 77861

Numerical Simulation Studies of Thermally-Induced Gas Production From Hydrate Accumulations With No Free Gas Zones at the Mallik Site, Mackenzie Delta, Canada

G.J. Moridis, SPE, Lawrence Berkeley National Laboratory, University of California

This paper was prepared for presentation at the SPE Asia Pacific Oil and Gas Conference and Exhibition held in Melbourne, Australia, 8—10 October 2002.

Abstract

The Mallik site represents an onshore permafrost-associated methane hydrate accumulation in the Mackenzie Delta, Northwest Territories, Canada. This study focuses on gas production at the Mallik site from hydrate deposits that are underlain by either a free water zone or by an impermeable boundary. The production analysis was conducted using a numerical simulator that can model the non-isothermal CH_4 release, phase behavior and flow under conditions typical of CH_4-hydrate deposits by solving the coupled equations of mass and heat balance. The simulator can describe any combination of the possible dissociation mechanisms (i.e., depressurization, thermal stimulation, salting-out effects and inhibitor effects). Accumulations with a CH_4-hydrate saturation of at least 50% were studied. Dissociation was induced mainly by a combination of thermal stimulation and depressurization as hot fluids circulated between injection and production wells. The effects of salinity and of pressure changes at the wells were also accounted for. The production strategy resulted in a zero net water production. The simulation results indicated that the amounts of CH_4 released from the dissociating hydrate deposits is sensitive to the hydrate saturation, the initial temperature, the specific enthalpy and the flow rate of the circulating fluids.

Introduction

Background. Gas hydrates are solid crystalline compounds in which gas molecules are encaged inside the lattices of ice crystals. Vast amounts of hydrocarbons are trapped in hydrate deposits[1]. Such deposits exist under favorable thermodynamic conditions that occur in two distinctly different types of geologic formations where the necessary low temperatures and high pressures exist: in the permafrost and in deep ocean sediments.

Current estimates of the worldwide quantity of hydrocarbon gas hydrates range between 10^{15} to 10^{18} m^3. Even the most conservative estimates of the total quantity of gas in hydrates may surpass by a factor of two the energy content of the total fuel fossil reserves recoverable by conventional methods[1]. The magnitude of this resource could make hydrate reservoirs a substantial future energy resource. Although the current energy economics cannot support gas production from hydrate accumulations, their potential clearly demands evaluation.

The Mallik site represents an onshore permafrost-associated methane hydrate accumulation in the Mackenzie Delta, Northwest Territories, Canada. A significant body of literature[2] on both the geology and the hydrate accumulations at the site became available following an 1150 m deep gas hydrate research well that was drilled in 1998. The objective of this study is to develop and evaluate strategies for gas production at the Mallik site from hydrate deposits that lack an underlying free gas zone. Thus, the hydrate intervals in this study are underlain by either a free water zone or by an impermeable boundary, and are particularly challenging because of high water production and/or adverse permeability conditions.

The numerical model. The numerical studies of gas production in this paper were conducted using the TOUGH2 general-purpose simulator[3] for multi-component, multiphase fluid and heat flow and transport in the subsurface with the EOSHYDR2 module[4,5]. By solving the coupled equations of mass and heat balance, EOSHYDR2 models the behavior of methane-bearing binary hydrates that are formed or dissociate in porous media according to the general reaction equation:

$$\chi_m[CH_4 \cdot n_m H_2O] \cdot \chi_G[G \cdot n_G H_2O] = \chi_m CH_4 + \chi_G G + (n_m + n_G) H_2O$$

where G is the second hydrate-forming gas, n is the hydration number, χ is the mole fraction in the binary hydrate, and the subscripts m and G denote the methane and the second gas, respectively. Obviously, $\chi_m + \chi_v = 1$. The gas G can be one of CO_2, H_2S, N_2, or another gaseous alkane C_vH_{2v+2} ($v = 2,3,4$).

Although χ_m often exceeds 95% in natural hydrates, the second gas G cannot be ignored because it can have a significant effect on the hydration pressure and temperature of the system[1]. EOSHYDR2 can describe the non-isothermal hydrate formation and/or dissociation, gas release, phase behavior, and fluid and heat flow under conditions typical of methane-bearing binary hydrate deposits (i.e., in the permafrost and in deep ocean sediments).

EOSHYDR2 includes both equilibrium and a kinetic model of gas hydrate formation and dissociation. The model accounts for heat and up to eight mass components: hydrate, water, native methane and methane from the hydrate dissociation, a second hydrate-forming gas (native and from dissociation), salt, and a water-soluble inhibitor (such as an alcohol). The mass components are distributed among four phases, i.e., a gas phase, a liquid phase, and two solid immobile phases: an ice phase and the hydrate phase. The thermophysical properties of the various mass components can be described at temperatures as low as —110°C. Dissociation, phase changes and the corresponding thermal effects are accounted for, as are the effects of salt and hydrate inhibitors. The model can describe gas hydrate dissociation involving any combination of the possible dissociation mechanisms (i.e., depressurization, thermal stimulation, as well as inhibitor and salting-out effects).

The Hydrate Zones of Study

Although this study focuses on gas production from deposits at the Mallik area, it should be noted that the analysis is not site-specific but applicable to any other hydrate accumulation with similar initial phase distribution (i.e., water and hydrate saturation) characteristics. The Mallik hydrate zones were selected because it is practically the only site for which sufficiently reliable field data are available. The two hydrate zones investigated in this study are referred to as Zones A and B.

Zone A. The hydrate layer in Zone A is 16 m thick, extends from —899 m to —915 m, and is underlain by 2-m-thick water-saturated layer. The hydrate and water saturations in the hydrate interval are S_H = 0.8 and S_w = 0.2, respectively, i.e., there is no free gas in this system. At the bottom of the hydrate interval, the pressure P = 9 MPa and the temperature T = 7.5 °C. The hydrate interval is capped by a tight and relatively thick gas-hydrate-bearing sandstone sequence with varying gas-hydrate saturations that acts as a no-flow boundary. Similarly, the water-saturated interval is underlain by a 2-m-thick low-porosity (ϕ<2%) sandstone that is assumed to act as a flow boundary. Zone A and its top and bottom boundaries are assumed to extend uniformly over a large area.

Zone B. This zone is characterized by the absence of any layers of mobile gas or water, the pore space being occupied primarily by gas hydrate and water (mostly immobile). Thus, this zone consists entirely of a hydrate system that is not in contact with a flowing water or gas interval. The hydrate layer extends from —1081 m to —1091 m, is assumed areally uniform, and has a uniform S_H = 0.8 (the rest being water). The pressure and temperature at the bottom of Zone B are P = 10.74 MPa and T = 7.5 °C. Zone B is capped by a relatively thick siltstone sequence, and is underlain by a relatively thick gas-hydrate-bearing sandstone sequence with varying gas-hydrate saturations. Both these two bounding formations are considered no-flow boundaries.

Properties and characteristics. In both zones the porosity (ϕ = 0.28), the intrinsic permeability (k = 20 mD), the thermal conductivity (k_θ = 1.5 W/m °C), the rock specific heat (C_R = 800 J/kg °C), and the hydrate specific heat (C_H = 1600 J/kg °C) were assumed to be the same. The regional plunge along the crest of the Mallik structure was not considered in the simulations because of the very shallow dip angle (2 degrees to the northwest). Relative permeabilities and capillary pressures were computed from the Parker et al. model[6], in which the irreducible aqueous and gas saturations were assumed to be S_{wr} = 0.2 and S_{gr} = 0.03, respectively. Because of the lack of a mobile gas phase and the adverse permeability to gas (intrinsic and relative), gas production from Zones A and B poses serious challenges.

Assumptions. Some general assumptions were made in all the simulations. The temperature distribution was determined by using the known temperature at particular points in the profile, and applying a heat flux corresponding to the geothermal gradient of 0.03 °C/m to the bottom of the simulated domain. The pressure distribution followed the hydrostatic gradient. The gas hydrate was assumed to be a simple methane-hydrate (i.e., χ_m = 1), an assumption supported by the gas composition studies from the site[2] that indicate $\chi_m \geq 0.98$. Finally, the dissociation of the hydrates was described by an equilibrium process. This is a valid assumption in cases of significant dissociation driving forces, such as a large depressurization or a strong thermal stimulation (both of which are involved in the proposed approach). Under these conditions, dissociation can be very rapid (and even explosive)[7].

It is important to indicate that the results discussed here should not be viewed as an attempt to provide definitive predictive answers to the problem of gas production from dissociating hydrates. The focus of the analysis is the determination of the relative importance and contributions of the various processes involved in dissociation, and the sensitivity of gas production to various reservoir conditions and operating parameters. This cautious approach of concentrating more on the relative rather than the absolute system performance is more appropriate, given the considerable uncertainties in the quantitative description of some fundamental processes involved in the dissociation of naturally-occurring hydrates[5,8].

Simulation of Production From Zone A

The numerical system. In all the simulations of production from Zone A, production and injection wells were arranged in a conventional five-spot pattern (Figure 1). The injected fluid was hot water because the parametric study of McGuire[9] indicated that when steam is injected, the amount of produced gas is less than the estimated fuel consumption. Hot water was injected into the center-well of the five-spot pattern, and reservoir fluids (i.e., water and gas from dissociation) were produced from the four production wells at rates determined by the prevailing relative permeabilities. The obvious advantage of this scheme is that it combines the two most important mechanisms of hydrate dissociation, i.e., depressurization at the production well, and thermal stimulation at the injection well. The lack of any free gas in Zone A guaranteed that the hydrate was the only possible source of any produced gas.

In an effort to focus the thermal stimulation and depressurization effects in the vicinity of the hydrate interface, the injection and production wells were completed in the top 1-m of the free-water zone underlying the gas hydrate layer. This configuration offered the additional advantage of limiting mixing of the injected hot water with the colder native reservoir water, while maximizing the thermal advantages of buoyancy that tended to concentrate the warmer water immediately below the hydrate interface. To take advantage of the gas buoyancy and the receding hydrate interface in its vicinity, the production well was also completed in the entire hydrate interval. However, this well interval did not contribute practically any fluids in the early stages of gas production because of adverse relative permeability conditions.

The selection of the five-spot multi-well production scheme was based on earlier work[10] that had indicated the advantages of multi-well systems over single wells. An additional reason was provided by the potential of this scheme to minimize water production, the disposal of which may pose environmental and economic challenges. In the proposed scheme, the injection and production rates were initially equal, and the produced fluid was initially 100% water. As dissociation progressed and gas began to appear in the production stream, the injection rate of the hot water was maintained equal to that of the produced water. Thus, the produced water was heated to the desired temperature and then reinjected, and the water injection rate was less than the rate of fluid production. This approach eliminated the potential environmental (and the corresponding economic) problems posed by the production of undesirable water, while minimizing the energy costs for the heating of the warmer reinjected water.

The water released during dissociation continuously dilutes the salinity of the native reservoir water. Because this is a localized phenomenon concentrated where flow (and, under the conditions of the proposed scheme, maximum dissociation) occurs, and the flowing water is recirculated through reinjection, salinity could not be ignored in this analysis. Note that the salinity level in the pore water can be significant, causing a 1.4 ^{o}C decrease in the dissociation temperature[2] at the prevailing pressure in Zone A.

The numerical grid. Because of symmetry, only a quarter of the domain was simulated using a 3-D Cartesian system. The side of the simulated quadrant was 30 m. The domain was discretized in 46x46x33 unequally spaced subdivisions in (x,y,z), resulting in a total of 69,828 gridblocks. Five equations (i.e., components) were considered (CH_4, H_2O, hydrate, salt, and heat) in each gridblock, leading to a system of 349,140 simultaneous equations. The large size and the complexity of the simulated system made the solution of the problem of production from Zone A very computationally demanding.

The base case. In this section and in all subsequent discussions, production and injection rates are based on the simulated quadrant of the five-spot pattern in Figure 1 (corresponding to 1/4th of the rates in the full system). In the base case, the initial water injection and production rate was Q = 2400 kg/day, and the injection temperature T_w = 50 ^{o}C.

There are two possible sources of the evolving gas: CH_4 originating from the depressurization-induced dissociation of hydrates in the vicinity of the production well (hereafter referred to as D-gas), and CH_4 from the thermally-induced dissociation of hydrates in the vicinity of the hot-water injection well (hereafter referred to as T-gas). These two gas streams are tracked separately. Note that it is impossible to completely separate pressure and thermal effects during dissociation: thermal changes will occur during depressurization-induced dissociation in response to the endothermic nature of the reaction, and the dissociation temperature will change in the vicinity of hot-water injection in response to the elevated pressure.

Figure 2 shows the cumulative gas release in Zone A over a 90-day period, and describes explicitly the contributions of depressurization and thermal stimulation. As expected, D-gas emerges earlier than T-gas because of the speed of propagation of the pressure wave and the significant thermal inertia of hydrate-impregnated media (hydrate being a relative thermal insulator). However, the pressure drop due to fluid withdrawal (the driving force of depressurization-induced hydrate dissociation) is relatively small, and is further hampered by a temperature decline in the vicinity of the production well (steeper before the hot water front arrives at the production well). This is caused by the endothermic nature of the hydrate dissociation reaction, and leads to an increase in the hydrate dissociation pressure, thus making hydrate dissociation progressively more difficult. The result is that the contribution of T-gas overtakes that of D-gas at an early stage.

The pressure distribution in Zone A on the plane that passes by the injection and the production wells at t=90 days is shown in Figure 3. The low-pressure region in the vicinity of the production well is clearly identified. The corresponding temperature distribution is shown in Figures 4 (near the

injection well) and 5 (near the production well), while Figure 6 presents the hydrate saturation distribution.

The thermal inertia of the hydrate-impregnated porous medium is demonstrated in Figure 4, which shows limited penetration of the thermal front into the hydrate layer. The cooling effect of depressurization-induced dissociation (due to the endothermic nature of the reaction) is shown in Figure 5, in which the area immediately above the free-water zone exhibits lower temperatures.

The hydrate saturation distribution in Figure 6 is characterized by a sharp hydrate interface (demonstrated by the bunching of the saturation contour lines). This was expected because the high initial hydrate saturation results in a very low relative permeability. Thus, for thermal dissociation, advection-driven heating is limited, conduction (a slow process) is important, and the corresponding thermal dissociation occurs over a very narrow zone at the hydrate interface. Additionally, the very low permeability limits the depressurization effect to a narrow zone at the interface. The result is dissociation that has the characteristics of an interface process. Lower hydrate saturations lead to higher fluid permeabilities and a more volume-based dissociation process. The hydrate saturation distribution in Figure 6 is consistent with the pressure and temperature distributions in Figures 3 to 5. Note the flatness of the bottom of the receding hydrate interface near the production well, which corresponds to an expanded (after the hydrate dissociation) free-water zone.

The cumulative gas production from the production well (and the corresponding mass fraction of the gas in the production stream) appear in Figure 7. Note that these are different from Figure 2 because of gas storage in the reservoir after dissociation. Comparison of Figures 7 and 2 indicates that the gas production and D-gas release are about equal at early times, but they begin to deviate as T-gas begins arriving at the production well. The arrival of T-gas is marked by a change in the slope of the cumulative gas production curve.

An important observation is that the produced gas represents a small fraction of the total produced mass (the rest being water), and does not exceed the 6% level during the 90-day simulation period. The gas mass fraction declines from an initial high, and then appears to stabilize at a level close to 2%. This behavior was expected because of the short distance the D-gas has to cover to reach the production well at early times. The possibility of this level rising after a longer injection-production period cannot be dismissed (as the expanding gas front from thermal dissociation reaches the production well), especially because the curve in Figure 7 shows faint signs of an upward trend. Unfortunately, the extremely demanding computational requirements dictated by the size and the complexity of the problem did not allow expansion of the study beyond the 90-day period.

Effect of the injection temperature T_w. These simulations differ from the ones for the base case in that the injection temperature T_w = 80 ^{o}C. Figure 8 shows the evolution of gas over time in Zone A. As in the base case, the volume of T-gas exceeds that of D-gas. As expected, the D-gas volume is not substantially different from that in the base case (see Figure 2). This observation conforms to expectations because the production rates (the driving force of depressurization) are the same in both cases. On the other hand, the T-gas volume is substantially larger than that in the base case. The increase is due to the larger specific enthalpy of the warmer water, leading to a deeper penetration of the thermal front (see Figure 9). However, the dependence of released gas on the injection temperature is sublinear because the large thermal inertia of the system results in higher temperatures in the vicinity of injection and larger temperature gradients, but not substantially deeper penetration.

The cumulative gas production and the corresponding gas mass fraction are shown in Figure 10, which shows patterns similar to those in Figure 7. Thus, at early times the gas production is roughly the same as the rate of D-gas release in the reservoir, and is later augmented by gas from thermal dissociation. The T-gas contribution to production is more substantial than in the base case due to the availability of larger volumes of such gas. The gas mass fraction shows a distinct upward trend that coincides with the arrival of T-gas at the production well.

Effect of the hydrate saturation S_H. These simulations differ from the ones for the base case in that the initial hydrate saturation S_H = 0.5. The cumulative gas volume release in Figure 11 shows the same pattern as in Figures 2 and 8, with the T-gas volume exceeding that of D-gas. The volume of the released CH_4, however, is lower than that in the other cases (in which S_H = 0.8). This is consistent with expectations. The difference is due to the smaller amounts of the gas source (i.e., the hydrate saturation).

Effect of the production rate Q. A change in the injection/production rate Q affects both the amount of heat available for thermal dissociation of the hydrate (at the injection well) and the pressure differential that drives depressurization (at the production well). This is evident in Figure 12, which shows a reduction in the gas released in zone A when Q is reduced to 1200 kg/day. In this case, the contribution of D-gas to the total gas release decreases because the lower fluid withdrawal rate affects depressurization more severely.

Further reduction of Q to 240 kg/day (1/10th the rate in the base case) results in the commensurate reduction in the released volume shown in Figure 12. Note that, unlike all previous cases (in which gas appears practically immediately), it takes almost 5 days for gas to begin evolving. This is due to the low rate Q, which is insufficient to provide the necessary heat (at the injection well) and pressure differential (at the production well) immediately upon the beginning of the operation.

Effect of the initial hydrate temperature T. Under the conditions of the proposed gas production scheme, higher initial hydrate (formation) temperature T is expected to lead to larger amounts of released gas because both thermal and

depressurization dissociation will be easier to attain. This is because a higher T reduces the considerable amount of heat needed in the wasteful process of raising the temperature of the hydrate (which has high heat capacity and low thermal conductivity) to the dissociation temperature. Additionally, a higher T allows depressurization-induced hydrate dissociation to proceed more effectively and for longer because (a) it corresponds to higher dissociation pressures (thus dissociating easier) and (b) provides a larger heat reservoir to cover the needs of the endothermic dissociation reaction (thus taking longer for the dissociation to decline because of cooling),

This is amply demonstrated by the simulation results of gas production when the temperature at the base of the hydrate interval is set to the hydration temperature T_H = 10 °C at the prevailing reservoir pressure. From Figure 13, it is evident that the effect on the released gas volume is rather dramatic. The cumulative released gas remains practically constant after 3-4 days, indicating complete dissociation of the hydrate in the five-spot quadrant. The released volumes are very large, and almost two orders of magnitude larger than the ones in all previous cases. Additionally, the contributions from depressurization and thermal stimulation show a different pattern: depressurization is by far the dominant contributor to gas release.

This is further confirmed by the evolution of the gas hydrate saturation on the injection-production well plane over time in Figure 14. The effect of depressurization is evident even at very early times. The depressurization-induced dissociation front propagates rapidly from the production well toward the injection well. It is remarkable that the last remaining intact hydrate region in Figure 14 at t = 1.5 days is located in the vicinity of the hot water injection well. This is rather counterintuitive, and is caused by the higher pressures near the injection well (which necessitate higher temperatures for dissociation) and the insulating thermal properties of the hydrates. The implication of these observations is that hydrate intervals at or in the vicinity of the dissociation temperature (i.e., the boundary of the hydrate stability zone) should be the obvious targets for hydrocarbon gas recovery because of the efficiency and speed of dissociation.

The proposed process transforms rapidly the simulated hydrate and water system into a gas and water system, from which fluids are withdrawn at a rate much slower than the gas generation rate. The cumulative gas production and the corresponding gas mass fraction in the production stream are shown in Figure 15, which indicates that far more gas is produced than in any other case. Additionally, the gas mass fraction follows the same general pattern as in Figures 7 and 10, but is significantly higher. This was expected because of the substantially larger amounts of released gas in the reservoir.

Production From Zone B

Flow-induced dissociation in Zone B is very difficult (and almost impossible initially) because of (a) the absence of a free (mobile) water or gas zone in contact with the hydrate interval, and (b) the very low permeability to the native water within the hydrate interval. At the initial S_H = 0.8, the water saturation S_w = 0.2 is at the irreducible level and the water relative permeability is zero. Under these conditions, the effectiveness of both depressurization and thermal stimulation as dissociation mechanisms is severely restricted because the pressure front cannot advance deeply into the hydrate zone, and heat transfer is limited to conduction only (a slow process in the insulating hydrates). Production from such non-flowing systems using hot water circulation in the wellbore was studied by Moridis *et al.*[7,10], who investigated the relative importance of various reservoir properties and operation parameters on gas recovery.

In the present study, the effort is focused on enhancing gas production through dissociation by adding the component of flow and heat advection to the process. This is possible only if the hydrate layer is fractured. Single well systems in continuous depressurization or huff-and-puff processes (that combine thermal, inhibitor and depressurization effects) were not addressed because of their limited effectiveness (a result of the very low volume of the fractures) and the possibility of self-healing fractures in the hydrates during cooling in depressurization-induced dissociation.

Thus, the studies of gas recovery from Zone B involved two-well systems (an injection and a production well) connected through fractures. In all the simulation of production from Zone A, the production and injection wells were located on the same fracture plane. Note that this and all other fracture-related properties in this study are significant assumptions, the validity of which is currently unknown given the existing knowledge gaps in the characteristics of hydrate fracturing.

Hot water was injected into the injection well, and reservoir fluids (i.e., water and gas) were produced from the production well at rates determined by the prevailing relative permeabilities. As in the case of Zone A, this scheme aimed to combine the advantages of two most important mechanisms of hydrate dissociation (i.e., depressurization at the production well, and thermal stimulation at the injection well). The initial phase distribution guaranteed the hydrates to be the exclusive source of any CH_4 gas evolving during the study.

In the simulations of Zone B, the injection and production wells were completed in the entire gas hydrate interval, and were spaced 30 m apart. The fractures were assumed to have a uniform aperture, to be fully saturated with mobile water (S_w = 1), to extend throughout the 10-m thickness of the hydrate layer without extending into the top and bottom bounding formations, and to extend 4 m past the wells in the x direction (see Figure 16). The fracture intrinsic permeability was k = 1000 mD. The production approach was the same as in Zone A. The injection and production rates were initially equal (and the produced fluid was initially 100% water). The water injection rate was equal to the time-variable rate of water production. Thus, the produced water was heated to the desired temperature and then reinjected, and the water injection rate was less than the rate of fluid production.

The numerical grid. Because of symmetry, only half the domain was simulated using a 2-D Cartesian areal system with a uniform thickness of Δz = 10 m. The dimensions of the simulated domain are shown in Figure 16. The domain was discretized in 120x44 unequally spaced subdivisions in (x,y), resulting in a total of 5720 gridblocks, of which 5504 were active and the remaining represented constant conditions at the x and y boundaries of the domain. The first subdivision in y corresponded to the fracture, which was assumed to have an aperture of $5x10^{-4}$ m.

The same five components discussed in Zone A were considered (CH_4, H_2O, hydrate, salt, and heat) here, leading to a system of 27,520 simultaneous equations. Heat losses into the underlying and overlying boundaries were accounted for using the semianalytical solution option available in TOUGH2[3]. Note that although the number of equations involved in Zone B was less than a 10^{th} of that in Zone A, the execution times were considerably longer because of the mathematical challenges posed by the fracture and the initial absence of flowing zones.

Water injection. In the simulations of Zone B, production and injection rates are based on the half-domain shown in Figure 16 (corresponding to half the rates in the full system). For the reasons discussed in Zone A, the initial injection fluid was hot water at a rate of Q = 120 kg/day and at a temperature T_w = 50 ^{o}C. Water was initially produced at the same rate from the production well. This low injection/production rate was selected to avoid possible (a) fracturing of the bounding formations (due to excessive pressures at the injection well) and subsequent fluid loss, and (b) cavitation (at the production well) if the system is incapable of supplying the flow rate imposed in the simulations. Both of those potential problems can arise because of the near-impermeability of the system and the very low fracture volumes.

Figure 17 shows the pressure distribution in the fracture at t = 10 days (at which time pressure has stabilized), and indicates that the selected rate is not expected to cause any serious problems. The corresponding temperature distribution in the reservoir in Figure 18 shows the limited extent of the volume affected by the hot water injection. This limited extent was expected because of the low injection rate, the relatively low specific enthalpy of the injected water, and the insulating behavior of the hydrates. The obvious implication is that, for effective dissociation, higher specific enthalpies are needed.

This is further confirmed by Figure 19, which shows the cumulative gas release in Zone B over a 90-day period. The released volumes are significantly smaller than those released in the hydrate dissociation from Zone A. All the gas evolving in the system originates from thermal dissociation because the production rate is insufficient to effect any depressurization-induced gas production. Thus, in this approach, higher injection/production rates are desirable, but the possibility of fracturing the bounding formations has to be considered.

The cumulative gas production at the well in Figure 19 shows a delay in the appearance of gas. This was expected because of the absence of any depressurization-originating CH_4 and of the distance the thermally released gas has to travel along the fracture before appearing at the production well.

Steam injection. In these simulations, the conditions were different from the water injection case in two respects. The injected fluid was superheated steam with a specific enthalpy corresponding to a pressure of 10 MPa and a temperature of 400 ^{o}C. Additionally, the initial injection/production rate was increased to Q = 240 kg/day.

Figure 17 shows the pressure distribution in the fracture. Note the reduction in depressurization (indicated by a flattening of the pressure distribution in the vicinity of the production well) caused by dissociation-driven gas release. The increase in the pressure at the injection well is much smaller than what the doubling of the injection rate would suggest (though it is unknown if it exceeds the fracture pressure of the bounding layers). The effect can be further mitigated if the compressibility of naturally occurring hydrates (assumed zero in the simulations) is significant.

The cumulative gas release in Figure 20 shows a drastically different behavior than that for the water injection in Figure 19. In this case, the released volumes are large, and depressurization is the main contributor to gas production. This was made possible by the larger production rate, which lowers pressure below the dissociation threshold.

The cumulative gas production at the well in Figure 20 shows an almost immediate appearance of gas at the production well. This is consistent with the large D-gas volumes in the vicinity of the production well. The hydrate saturation distribution at early times (t † 2 days) in Figure 21 shows explicitly the rapid dissociation pattern inferred from the cumulative gas production.

Summary and Discussion

The Mallik site represents an onshore permafrost-associated methane hydrate accumulation in the Mackenzie Delta, Northwest Territories, Canada, and is characterized by several hydrate intervals. This study focuses on gas production from hydrate deposits that are underlain by either a free water zone or by an impermeable boundary. These are some of the most challenging targets for gas recovery because of adverse permeability and the thermal properties of hydrates. Although this investigation focuses on gas production from deposits at the Mallik area (because of the availability of sufficiently reliable data), the analysis is generic in that it is applicable to any other hydrate accumulation with similar initial phase distribution (i.e., water and hydrate saturation) characteristics.

The simulation studies were conducted using the TOUGH2 simulator[3] with the EOSHYDR2 module[5]. This module is designed to model the non-isothermal gas release, phase behavior and flow under the conditions of the common methane hydrate deposits (i.e., binary hydrates involving

methane in the permafrost and in deep ocean sediments) by solving the coupled equations of mass and heat balance. As with all other members of the TOUGH2 family of codes, EOSHYDR2 can handle multi-dimensional flow domains and Cartesian, cylindrical or irregular grids in porous and fractured media. The model accounts for up to four phases (gas phase, liquid phase, ice phase and hydrate phase), up to nine components (CH_4-hydrate, water, native and dissociated CH_4, a second native and dissociated hydrate-forming gas, salt, water-soluble inhibitors and heat), and can describe all possible hydrate dissociation mechanisms, i.e., depressurization, thermal stimulation, salting-out effects and inhibitor-induced effects.

The two hydrate zones investigated in this study lacked any initial free gas saturation. Zone A included a water-saturated layer (with no hydrates) underlying the hydrate interval, while the hydrate layer occupied the entire Zone B. Hydrate saturations in both zones were at least 50%, and the remainder of the pore space was occupied by water. Gas produced from these hydrate deposits was certain to have originated from the hydrates.

In Zone A, hot water was injected into the underlying water zone through injection wells, and reservoir fluids were withdrawn from the production wells of a five-spot pattern. The water produced from the production well was heated and reinjected into the injection well, resulting in a net zero withdrawal of water. Thus, potentially adverse environmental impacts of the produced water were eliminated, and the corresponding economic considerations were alleviated because of the elimination of the cost for water disposal and the reduction in the energy requirement for the heating of the reinjected water.

Because of high hydrate saturation, flow is impossible without fracturing in Zone B. In this case, a system of two wells connected through a common fracture was used. The approach in Zone B was similar to that in Zone A, and involved a zero net water withdrawal. Hot water and superheated steam were injected into the injection well, and reservoir fluids were withdrawn from the production well.

The results of the simulations indicate that, in Zone A, gas release in the reservoir increases with the specific heat of the injected water (a function of its temperature) because this increases the amount of heat available for dissociation. An increasing injection rate leads to larger gas releases because of increased thermal and depressurization-induced dissociation. Larger initial hydrate saturations lead to larger releases because of the availability of larger gas sources. The initial formation temperature may have a dramatic effect on the volume of the released gas. Hydrates at higher temperatures require substantially smaller depressurization and far less heat for dissociation.

The limited study of production from Zone B indicates that, despite the relatively large fracture permeabilities, the small fracture volumes in such systems may pose challenges. In the balanced injection/production regime proposed in this study, by minimizing injection rates to prevent potential fracturing of the bounding formation, it is possible to inhibit depressurization (an unwelcome development) if the pressure fails to fall below the dissociation threshold. To avoid this problem, the highest safe level of injection rate and the highest possible specific enthalpy of the injected fluid (e.g., by resorting to superheated steam) are possible mitigation strategies.

To complete this study, it is important to assess the impact of a number of other factors on gas release and recovery. These include the formation intrinsic permeability, the fracture area (in Zone B), the system thermal properties (conductivity and specific heat), and the relative permeability. Of those, relative permeability poses a particular challenge because there is no quantitative information on its behavior in hydrate-impregnated media. The thermal conductivity of the hydrate-bearing medium is known to have a significant effect on gas recovery[7,10] in conduction-driven dissociation, but its importance remains to be determined in advection-driven processes. It is expected that production is less sensitive to the rock and hydrate specific heats, and to the irreducible gas saturation, but this has not yet been demonstrated. Additionally, operational parameters (such as time-variable injection-production rates in fractured hydrates to take advantage of the increased hydrate-free volume and the corresponding larger permeability after dissociation) merit investigation.

Note that, while the pathway for a thorough study of hydrate behavior is rather evident, there are significant practical difficulties that slow the pace of such investigations. Among the most challenging are the extraordinarily large computational requirements for the study of such systems, necessitated by the complexity of the underlying physics and the need for fine discretization. Thus, even when using some of the most powerful computers, the simulations of the various production cases in Zones A and B can easily take days to whole weeks.

The most serious limitation, however, is the dearth of information on the fundamental properties of hydrate reservoirs and their field thermodynamic behavior. There are practically no reliable measurements of the permeability, porosity and saturation of natural hydrate deposits, while the understanding of the kinetic behavior of hydrates is at a very early stage[1]. Additionally, there are significant scientific challenges and knowledge gaps that must be addressed for numerical simulation to provide reliable predictions of gas production. These include the type of formation/dissociation reactions occurring in natural accumulations (equilibrium vs. kinetic), the values and temperature dependence of the corresponding parameters under field conditions, the hysteretic behavior between the formation and dissociation P-T equilibrium curves, the relative permeability in hydrate formations, hydrocarbon solubility near the hydration point, hydrate thermal properties, and the effect of the hydration number on the properties and behavior of hydrates. The fact that no representative undisturbed sample of natural hydrates has been obtained to-date indicates the magnitude of the problem.

Thus, at this stage, our ability to describe mathematically the hydrate system exceeds our knowledge of some basic processes that control their behavior. This should not be interpreted as lack of confidence in the role of numerical simulation. Even with the current lack of data, numerical simulation makes it possible to establish envelopes of possible solutions and to identify promising target zones of hydrates for development. This is the light under which the current study must be considered. With this approach in mind, the results discussed here should not be viewed as an attempt to provide definitive predictive answers to the problem of gas production from dissociating hydrates. Instead, the emphasis must be in the determination of the relative importance and contributions of the various processes involved in dissociation, and the sensitivity of gas production to various reservoir conditions and operating parameters, rather than in the absolute system performance.

Acknowledgement

This work was supported by the Assistant Secretary for Fossil Energy, Office of Natural Gas and Petroleum Technology, through the National Energy Technology Laboratory, under the U.S. Department of Energy, Contract No. DE-AC03-76SF00098. The author is indebted to Stefan Finsterle and John Apps for their insightful review comments.

References

1. Sloan, E.D.: *Clathrate Hydrates of Natural Gases*, Marcel Dekker, Inc., New York, NY (1998)
2. Dallimore, S.R., Uchida, T., and Collett, T.S. (eds.): Scientific Results from JAPEX/JNOC/GSC Mallik 2L-38 Gas Hydrate Research Well, Mackenzie Delta, Northwest Territories, Canada , Geological Survey of Canada Bulletin 544 (1999).
3. Pruess, K., C. Oldenburg, and Moridis, G.: TOUGH2 User s Guide — Version 2.0 , Report LBL-43134, Lawrence Berkeley Laboratory, Berkeley, CA (1999).
4. Moridis, G.J., Apps, J., Prues, K., and Myer, L.: EOSHYDR: A TOUGH2 Module for CH4-Hydrate Release and Flow In the Subsurface , Report LBNL-42386, Lawrence Berkeley Laboratory, Berkeley, CA (1998).
5. Moridis, G.J.: Numerical Studies of Gas Production from Methane Hydrates , paper SPE 75691 presented at the 2002 SPE Gas Technology Symposium, Calgary, Alberta, Canada, April 30—May 2 (also Report LBNL-49765, Lawrence Berkeley National Laboratory, Berkeley, CA).
6. Parker, J.C., Lenhard, R.J., and Kuppusamy, T.: A Parametric Model for Constitutive Properties Governing Multiphase Flow in Porous Media , *Water Resour. Res.* (1976), **12**(1), 57.
7. Moridis, G.J., Collett, T.S., Dallimore, S.R., Satoh, T., Hancock, S., and Weatherhill, B.: Numerical Simulation Studies of Gas Production Scenarios From Hydrate Accumulations at the Mallik Site, Mackenzie Delta, Canada , *Proc*., 4th International Symposium on Gas Hydrates, Yokohama, Japan, June 19-23 (2002) 86 (also Report LBNL-49764, Lawrence Berkeley National Laboratory, Berkeley, CA).
8. Swinkels, W.A.M., and Drenth, R.J.J.: Thermal Reservoir Simulation Model of Production From Naturally Occurring Gas Hydrate Accumulations , *SPERE* (2000), **3**(6), 559.
9. McGuire, P.L.: Methane Hydrate Gas Production: An Assessment of Conventional Production Technology as Applied to Hydrate Recovery, Report LA-9102-MS, Los Alamos National Laboratory, Los Alamos, NM (1981).
10. Moridis, G.J., Collett, T.S., Dallimore, S.R., Satoh, T., Hancock, S., and Weatherhill, B.: Numerical Studies of Gas Production Scenarios From Several CH_4-Hydrate Accumulations at the Mallik Site, Mackenzie Delta, Canada , Report LBNL-50257, Lawrence Berkeley National Laboratory, Berkeley, CA (2002).

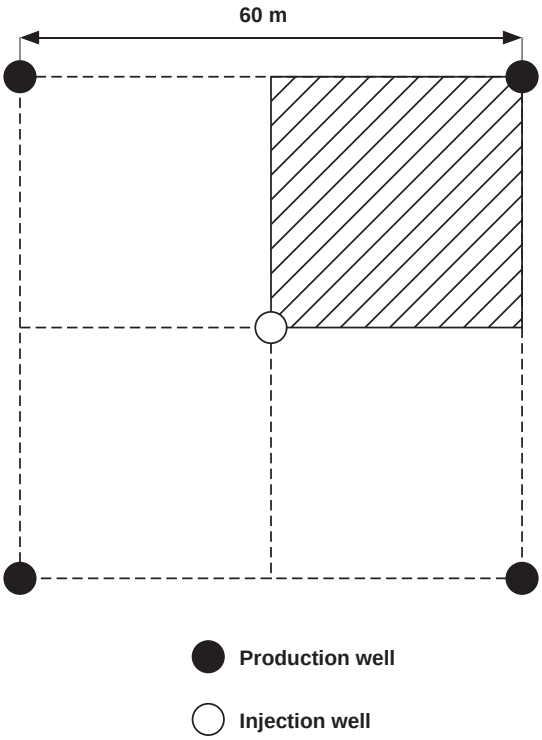

Figure 1 - Five-spot well pattern for modeling a 1/4 symmetry subdomain (shaded) in the simulations of Zone A.

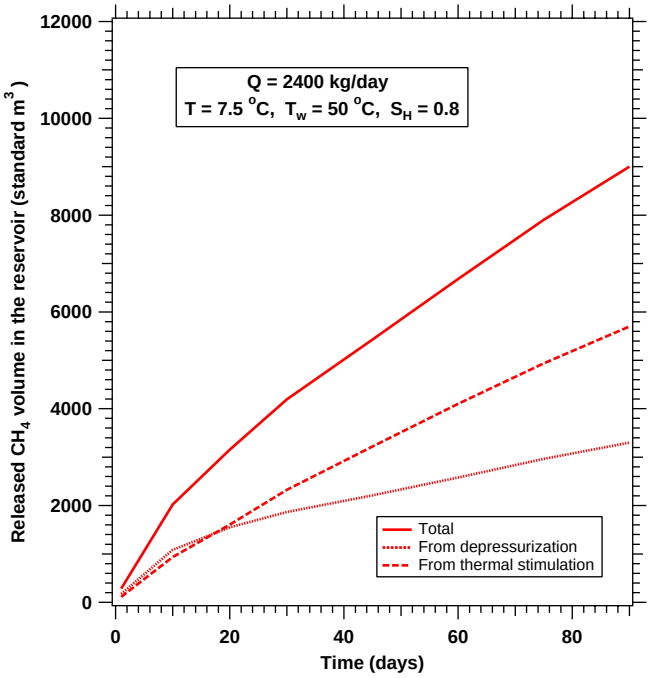

Figure 2 — Base case: cumulative gas release in Zone A. The contributions of gas from depressurization- and thermally-induced hydrate dissociation are described.

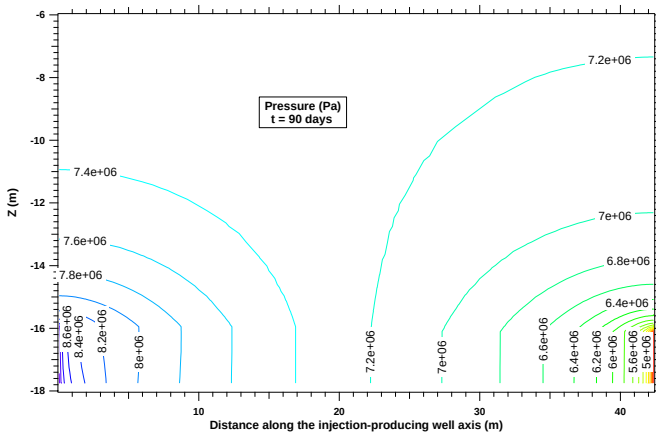

Figure 3 — Pressure distribution on the injection-production well plane at t = 90 days (base case, Zone A).

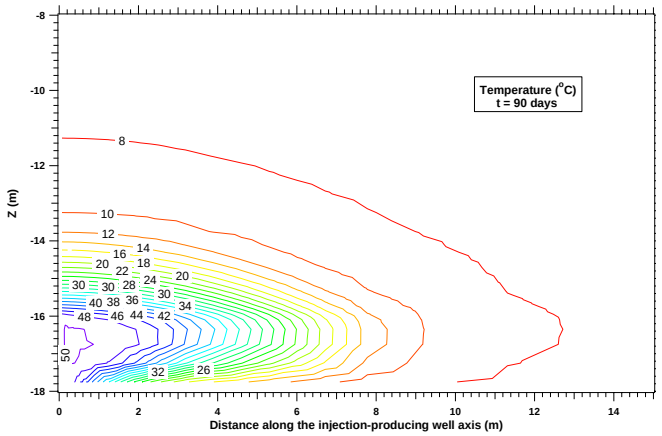

Figure 4 — Temperature distribution on the injection-production well plane at t = 90 days (base case, vicinity of the hot water injection well, Zone A).

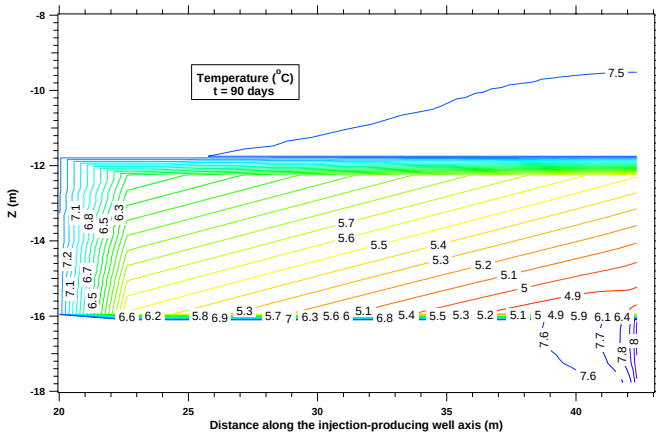

Figure 5 — Temperature distribution on the injection-production well plane at t = 90 days (base case, vicinity of the production well, Zone A).

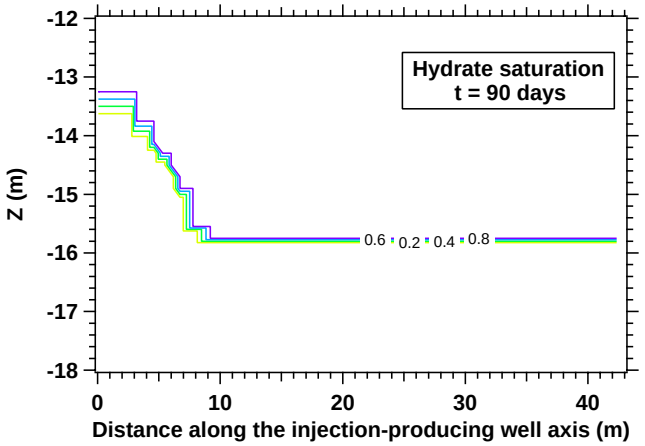

Figure 6 — Hydrate saturation distribution on the injection-production well plane axis at t = 90 days (base case, Zone A).

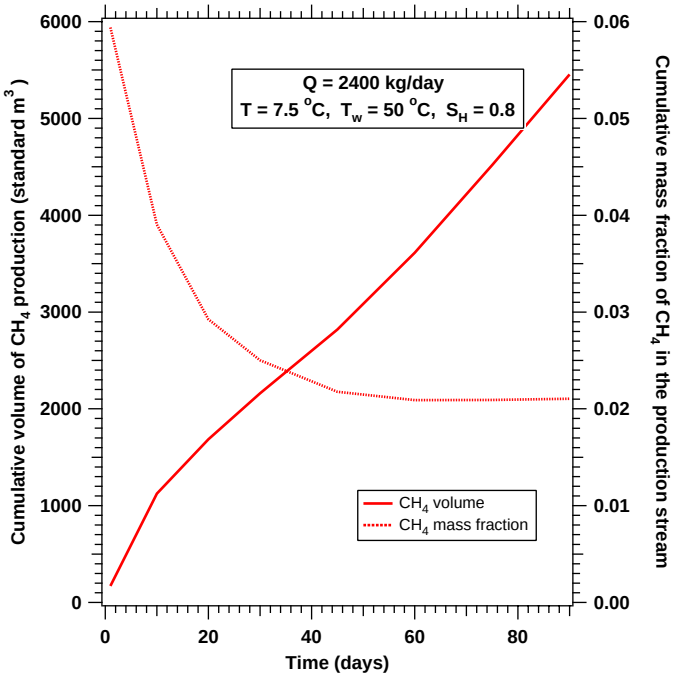

Figure 7 — Cumulative gas production and gas mass fraction in the production stream of the base case in Zone A.

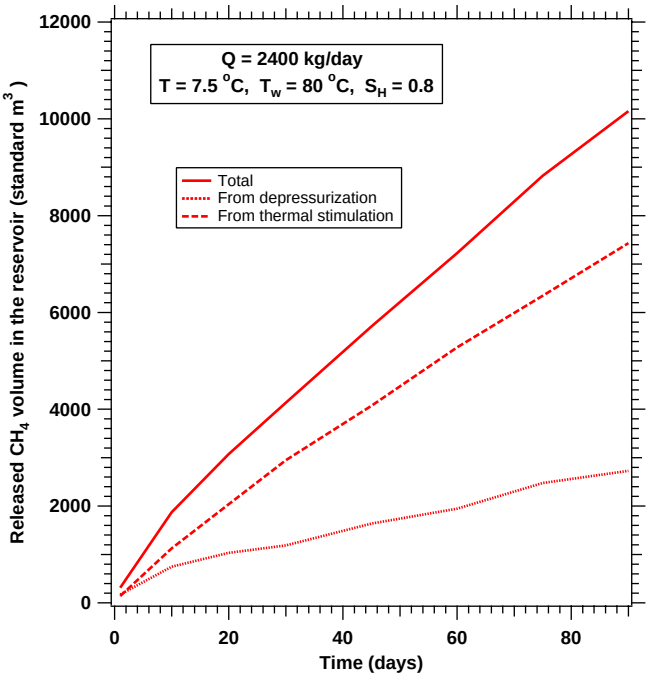

Figure 8 — Cumulative gas release in Zone A when T_W= 80 °C.

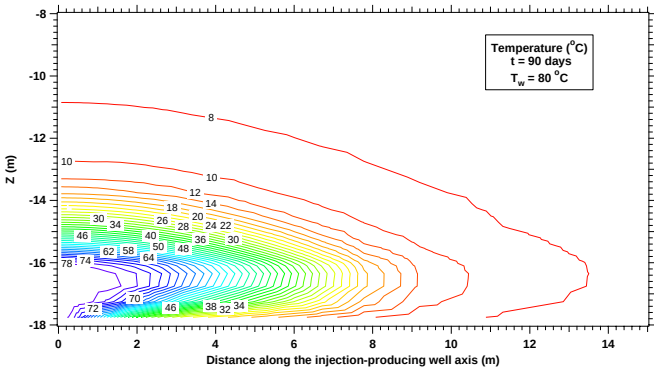

Figure 9 —Temperature distribution on the injection-production well plane at t = 90 days (T_W = 80 °C, vicinity of the hot water injection well, Zone A).

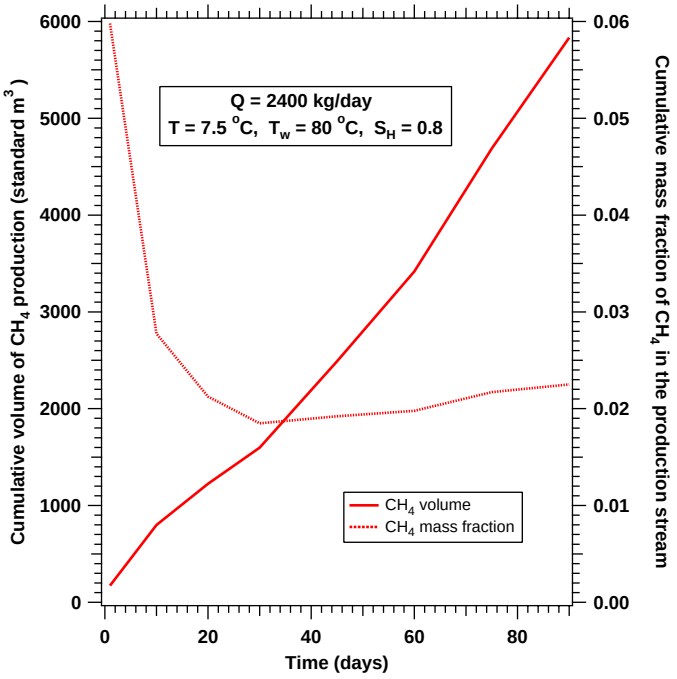

Figure 10 — Cumulative gas production and gas mass fraction in the production stream of the base case in Zone A.

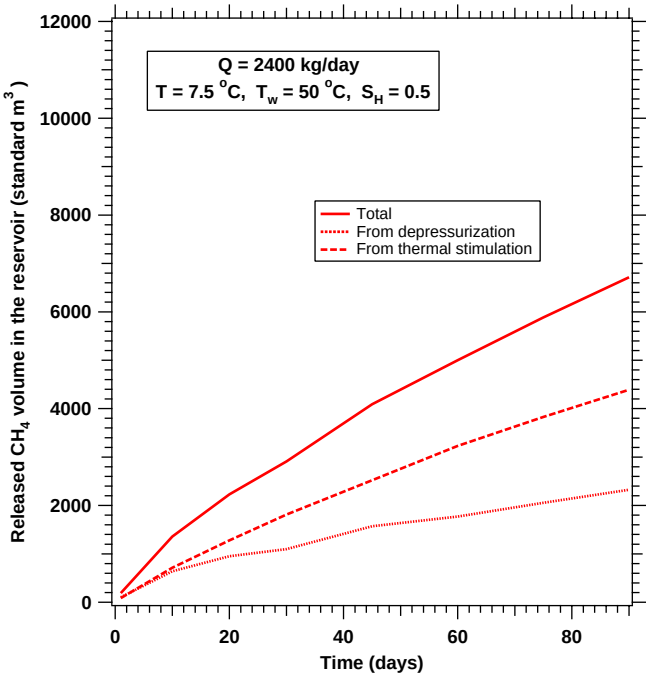

Figure 11 — Cumulative gas release in Zone A when S_H = 0.5.

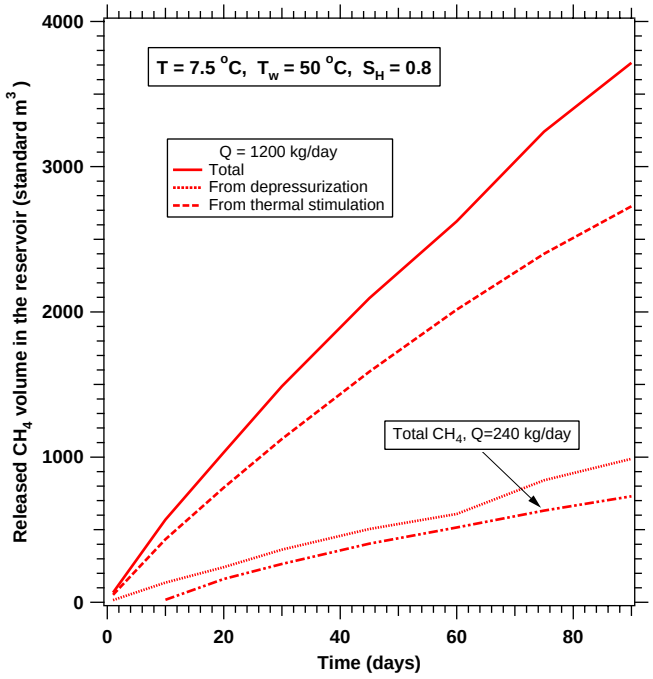

Figure 12 — Cumulative gas release in Zone A when Q = 1200 kg/day and Q = 240 kg/day.

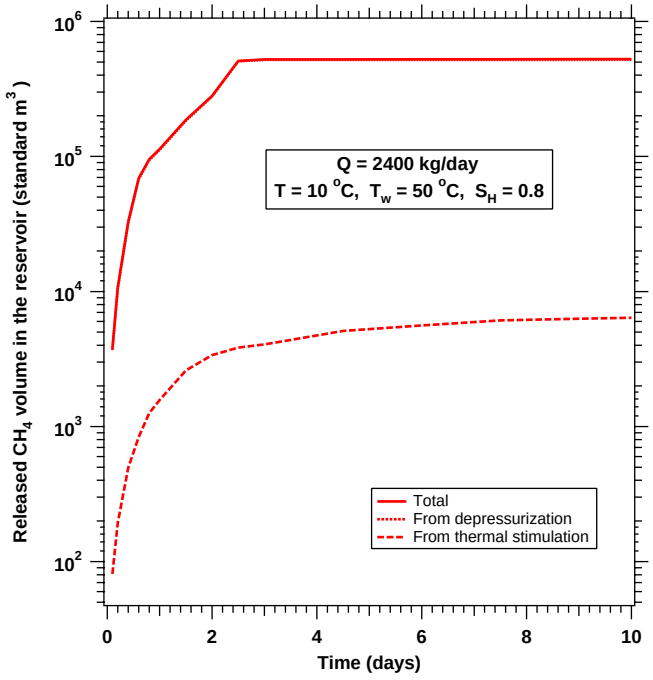

Figure 13 — Cumulative gas release in Zone A when T = 10°C (the curve for the D-gas release practically coincides with that for the total released gas).

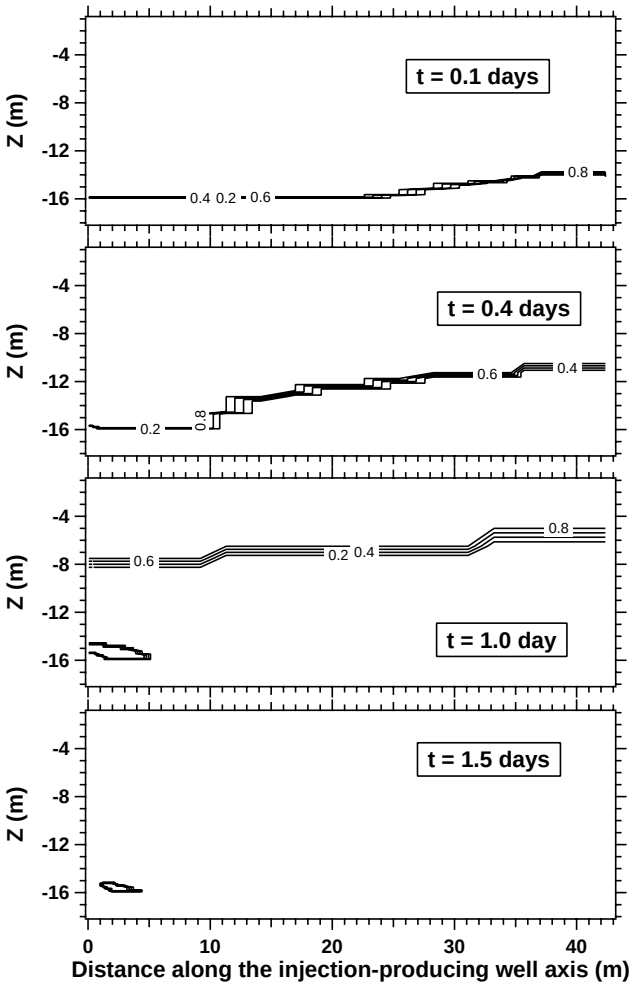

Figure 14 — Evolution of the hydrate saturation on the injection-production plane when T = 10 °C (Zone A).

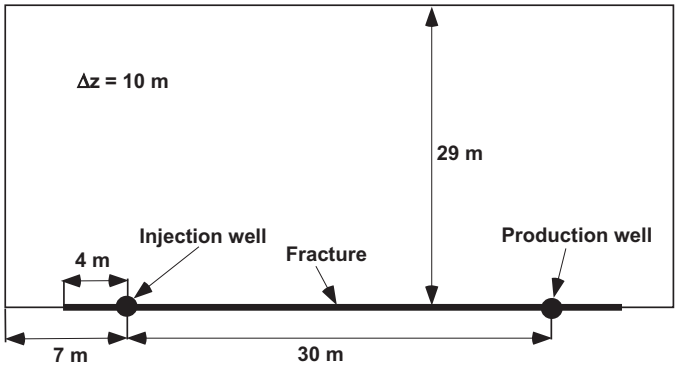

Figure 16 — A schematic of the areal configuration of the injection-production system in Zone B (not to scale).

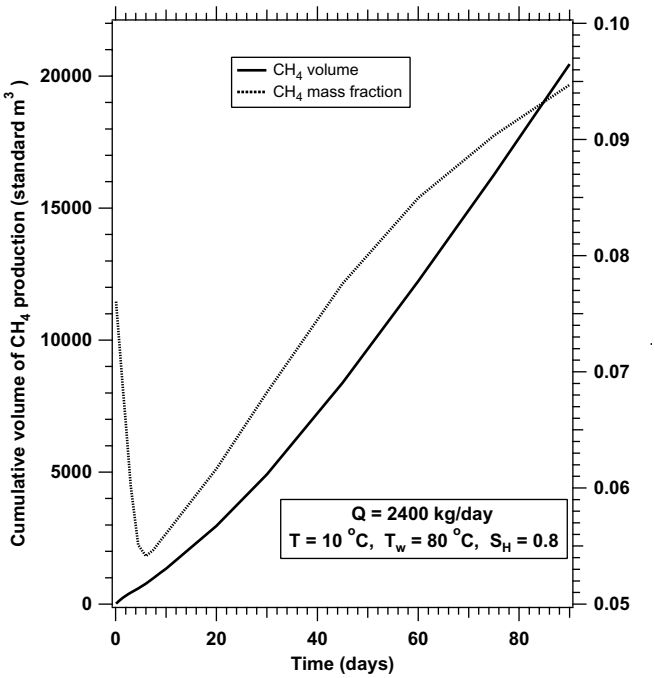

Figure 15 — Cumulative gas production and gas mass fraction in the production stream when T = 10 °C (Zone A).

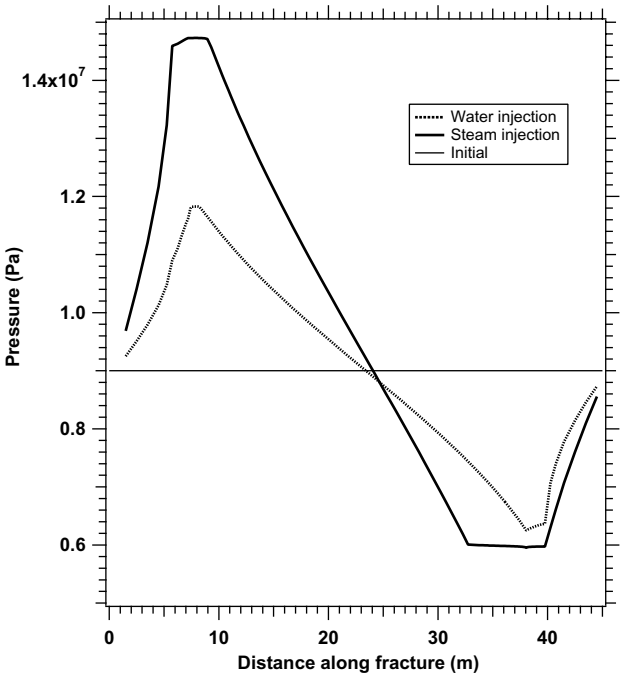

Figure 17 — Pressure distribution in the fracture of Zone B during water and steam injection (t = 10 days).

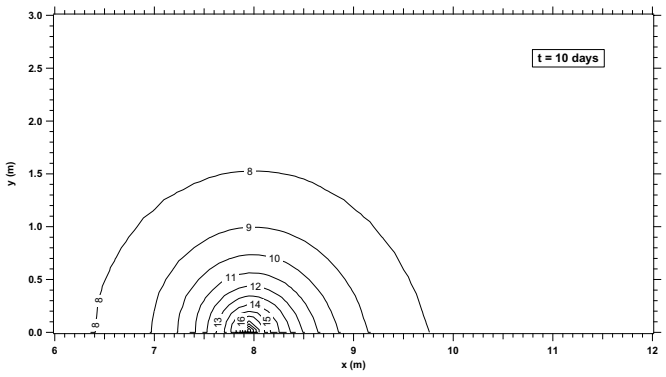

Figure 18 — Areal temperature distribution at t = 10 days in the vicinity of the injection well during water injection (Zone B).

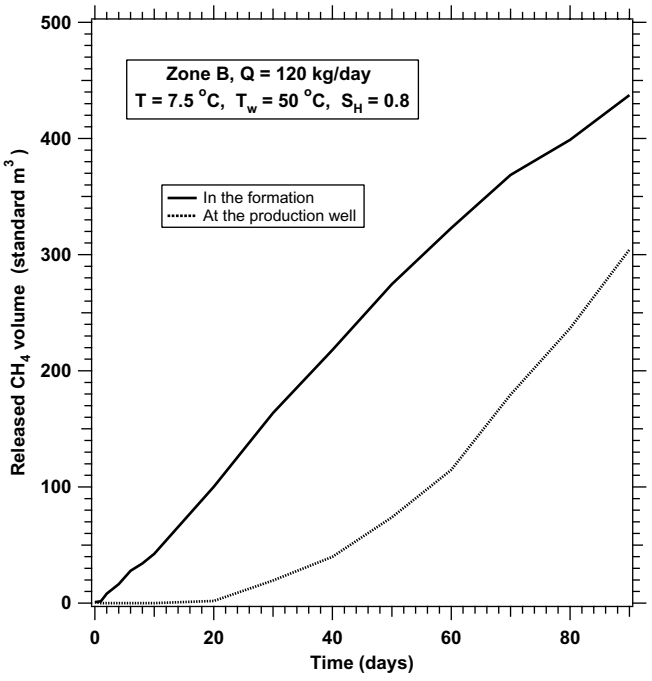

Figure 19 — Cumulative gas release in the reservoir and at the well during water injection (Zone B). Note that all the gas is originating from thermal dissociation.

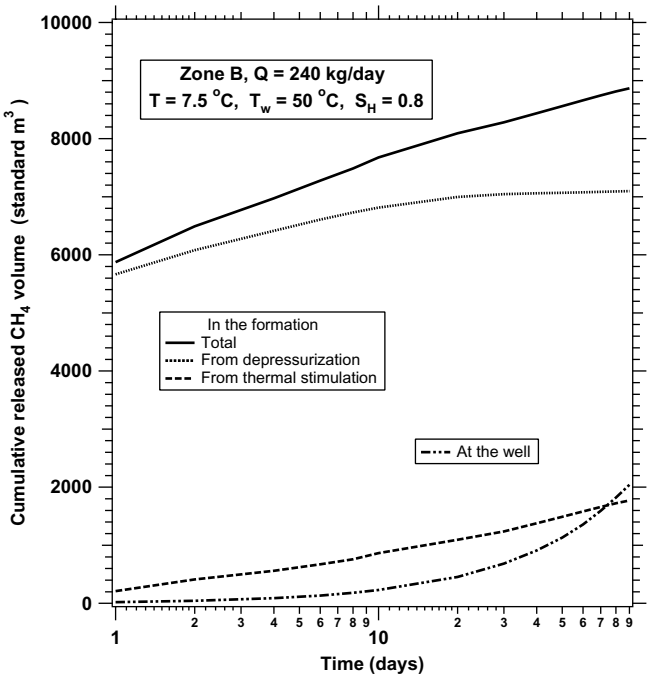

Figure 20 — Cumulative gas release in the reservoir and at the well during steam injection (Zone B).

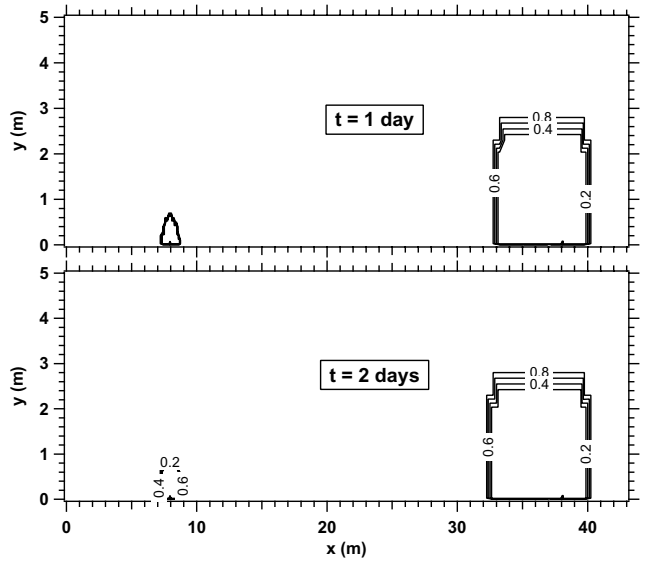

Figure 21 — Gas hydrate areal distribution during superheated steam injection (Zone B).